Atmos. Chem. Phys., 13, 10689–10701, 2013
www.atmos-chem-phys.net/13/10689/2013/
doi:10.5194/acp-13-10689-2013
© Author(s) 2013. CC Attribution 3.0 License.

Atmospheric Chemistry and Physics Open Access

The contribution of the strength and structure of extratropical cyclones to observed cloud–aerosol relationships

B. S. Grandey[1,2], **P. Stier**[1], **R. G. Grainger**[1], **and T. M. Wagner**[1]

[1]Atmospheric, Oceanic and Planetary Physics, Department of Physics, University of Oxford, Oxford, UK
[2]Singapore-MIT Alliance for Research and Technology, Singapore

Correspondence to: B. S. Grandey (benjamin@smart.mit.edu)

Received: 24 January 2013 – Published in Atmos. Chem. Phys. Discuss.: 7 May 2013
Revised: 19 September 2013 – Accepted: 5 October 2013 – Published: 4 November 2013

Abstract. Meteorological conditions may drive relationships between aerosol and cloud-related properties. It is important to account for the meteorological contribution to observed cloud–aerosol relationships in order to improve understanding of aerosol–cloud–climate interactions. A new method of investigating the contribution of meteorological covariation to observed cloud–aerosol relationships is introduced. Other studies have investigated the contribution of local meteorology to cloud–aerosol relationships. In this paper, a complimentary large-scale view is presented. Extratropical cyclones have been previously shown to affect satellite-retrieved aerosol optical depth (τ), due to enhanced emission of sea salt and sea surface brightness artefacts in regions of higher wind speed. Extratropical cyclones have also been shown to affect cloud-related properties such as cloud fraction (f_c) and cloud top temperature (T_{top}). Therefore, it seems plausible to hypothesise that extratropical cyclones may drive relationships between cloud-related properties and τ. In this paper, this hypothesis is investigated for extratropical cyclones, henceforth referred to as storms, over the Atlantic Ocean. MODerate resolution Imaging Spectroradiometer (MODIS) retrieved τ, f_c and T_{top} data are analysed using a storm-centric coordinate system centred on extratropical cyclones which have been tracked using European Centre for Medium Range Weather Forecasts (ECMWF) reanalysis 850 hPa relative vorticity data. The tracked relative vorticity (ω) is used as a measure of storm strength, while position in the storm-centric domain is used to account for storm structure. Relationships between the cloud-related properties and τ are measured by calculating regression slopes and correlations. The f_c–τ relationships are positive, while the T_{top}–τ relationships are negative. By shuffling the pairing of the cloud and τ data at each location in the storm-centric domain and within narrow ω bins, the contribution of storm strength and storm structure to the observed relationships can be investigated. It is found that storm strength and storm structure can explain only a small component of the relationships observed in the MODIS data. The primary causes for observed cloud–aerosol relationships are likely to be other factors such as retrieval errors, local meteorology or aerosol–cloud interactions.

1 Introduction

Much of the uncertainty in projections of future climate is associated with present-day aerosol radiative forcing (Andreae et al., 2005; Kiehl, 2007). Aerosol indirect effects on clouds represent an important part of the climate system, but large uncertainties remain regarding the size of these effects (Lohmann and Feichter, 2005; Forster et al., 2007).

Strong relationships between aerosol and cloud-related properties have been observed. For example, positive relationships between total cloud fraction (f_c) and aerosol optical depth (τ) exist in data retrieved from the MODerate resolution Imaging Spectroradiometer (MODIS) instrument (Koren et al., 2005; Kaufman et al., 2005; Grandey et al., 2013). Similarly, positive relationships between cloud top height and τ have also been observed (Koren et al., 2005).

Potentially, many causal mechanisms may be able to explain these observed relationships (Stevens and Feingold, 2009; Grandey et al., 2013). For example, meteorological conditions may drive relationships between aerosol and cloud-related properties. Ten-metre wind speeds can explain

a large part of observed f_c–τ correlations (Engström and Ekman, 2010). Additionally, covariation with humidity can lead to positive f_c–τ relationships (Quaas et al., 2010; Chand et al., 2012; Grandey et al., 2013). Most previous studies which consider potential meteorological contributions to observed aerosol–cloud relationships, including those mentioned above, have looked at simple local meteorological variables such as relative humidity and wind speed. Large-scale synoptic conditions are an important factor affecting local meteorology. Therefore, large-scale synoptic systems may lead to correlations between aerosols and clouds, potentially organising spatiotemporal patterns in cloud–aerosol relationships.

It is possible that the causal mechanisms driving cloud–aerosol relationships may vary between different regions. This paper focuses on relationships in the midlatitude storm tracks.

Many studies have shown that extratropical cyclones and fronts are major drivers of large-scale cloud-related properties (Lau and Crane, 1995, 1997; Norris and Iacobellis, 2005; Wang and Rogers, 2001; Chang and Song, 2006; Field and Wood, 2007; Field et al., 2008). The high wind speeds associated with extratropical cyclones can increase sea salt emission and introduce surface brightness artefacts to satellite retrievals, increasing the aerosol optical depth (Grandey et al., 2011). Since extratropical cyclones have been shown to affect cloud-related properties and τ, it seems credible to hypothesise that extratropical cyclones may drive relationships between cloud-related properties and τ. Here, the storm-centric compositing methodology is applied to the investigation of observed relationships between τ and f_c and between τ and cloud top temperature (T_{top}), a measure of cloud top height. The relative vorticity of each storm and position relative to the storm centre are considered in order to provide a simplified description of the large-scale forcing of aerosols and clouds by extratropical cyclones. The storm's relative vorticity is used as a measure of storm strength, while the position relative to the storm's centre allows the storm's spatial structure to be accounted for. The following question is considered in this paper: can relationships between aerosol and cloud-related properties be explained by considering simply the relative vorticity of extratropical cyclones and position relative to the storm's centre?

The data and methodology used are explained in Sect. 2. Results are presented and discussed in Sect. 3. Conclusions are summarised in Sect. 4.

2 Method

2.1 Data

This paper uses daytime data from the MODIS Science Team Collection 5 Atmosphere Level 2 Joint Product for the Aqua satellite (MYDATML2) (Platnick et al., 2003; Remer et al., 2005). These level 2 data have a temporal resolution of 5 min. In addition to the 10 km × 10 km aerosol optical depth (τ) data used in Grandey et al. (2011), this paper also uses 5 km × 5 km cloud fraction (f_c) and cloud top temperature (T_{top}) data. Liquid cloud top properties, such as liquid cloud droplet number concentration, are not investigated here. Strict ocean-retrieval-only masking is applied to the τ data only. Retrievals of f_c and T_{top} are likely to be far less sensitive to surface albedo changes between land and ocean, although the T_{top} of thin or broken clouds may sometimes be contaminated by surface emissivities which differ between land and ocean. As in Grandey et al. (2011), 6 hourly 1.5° × 1.5° ERA-Interim 850 hPa relative vorticity, zonal and meridional components of the 10 m wind and mean sea level pressure are also used. All data cover 2003–2007.

2.2 Storm-centric and all-conditions gridding

The storm-centric gridding methodology is almost identical to that explained in Grandey et al. (2011). Extratropical cyclones are tracked using TRACK (Hodges, 1995, 1999). TRACK has been configured to track ERA-Interim 850 hPa relative vorticity features associated with extratropical cyclones, henceforth referred to as storms. The tracked storm-centre 850 hPa relative vorticity (ω) provides a measure of the strength of the storm. Only storms which have $\omega > 1\times10^{-5}\,s^{-1}$, persist for at least 2 days and move a distance of more than 1000 km are considered. There is generally good agreement in tracked cyclone locations between different reanalysis data sets, with storm centre location disagreements of typically less than 2° (geodesic) (Hodges et al., 2011).

For each storm at each model time step, the ERA-Interim 10 m wind and mean sea level pressure data are regridded to a resolution of 200 km × 200 km on a 4000 km × 4000 km storm-centric domain centred on the tracked storm. There is generally greater uncertainty in the storm-centric 10 m winds and ω than there is in mean sea level pressure, a larger-scale field (Hodges et al., 2011). In order to find the storm locations and strengths at each MODIS overpass time, the storm locations and ω are interpolated to 5 min temporal resolution, using a parametric cubic spline with time as the parameter. If level 2 τ, f_c or T_{top} satellite-retrieved data exist within the 4000 km × 4000 km storm-centric domain, then the data are regridded to a resolution of 200 km × 200 km on the domain. 200 km × 200 km seems to be a reasonable choice of co-location scale for much of the aerosol–cloud interaction analysis. At this scale, the assumption of clear-sky τ being representative for the grid box should hold, such that the τ data generally can be assumed to be co-located with the f_c and T_{top} data, although individual pollution plumes may occur on smaller scales (Anderson et al., 2003; Weigum et al., 2012). It is worth noting that satellite-retrieved τ data are for clear-sky conditions, because aerosol retrievals require pixels that have been flagged as cloud-free, although some cloud contamination of τ may remain.

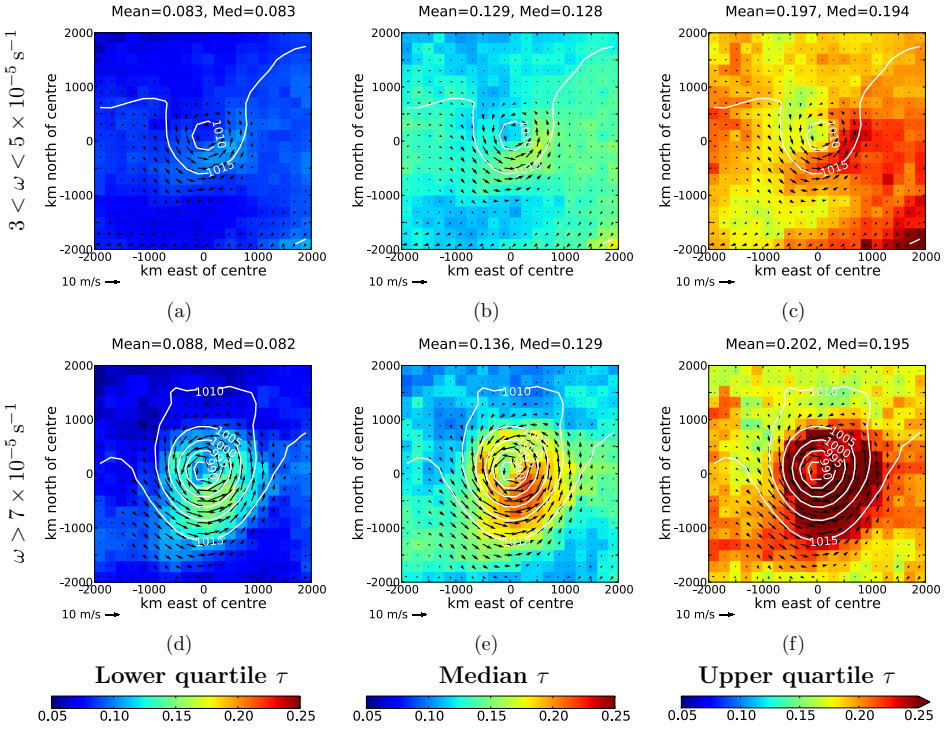

Fig. 1. Storm-centric **(a, d)** lower quartile, **(b, e)** median and **(c, f)** upper quartile composites of Aqua-MODIS aerosol optical depth (τ) for two 850 hPa relative vorticity (ω) ranges over the North Atlantic ocean. Median composites of ERA-Interim mean sea level pressure (p_0; white contours) and wind vectors (black arrows) are over-plotted. The wind vector scale is provided at the bottom left-hand edge of each composite. Positive meridional displacements are poleward of the storm centre. The data cover 2003–2007.

Alongside the storm-centric regridding, the data are also regridded with respect to storm tracks which have have been translated temporally by 1 yr, creating "all-conditions" data (Grandey et al., 2011). These all-conditions data should be representative of average conditions. They are blind as to whether or not a storm is present in the domain, but they retain the same seasonal and locational sampling as the storm-centric data.

Most of the results for North Atlantic ocean (NA; 50–10° W, 30–55° N) storms are shown and discussed in this paper. Some of the corresponding results for the South Atlantic ocean (SA; 50° W–10° E, 55–30° S) are shown in the Supplement. The SA results, which are generally similar to those for the NA, are also discussed briefly in the main body of this paper.

2.3 Composites of aerosol and cloud properties

In order to illustrate how τ, f_c and T_{top} change between weaker and stronger storms, median composites for a weaker relative vorticity range of $3 < \omega < 5 \times 10^{-5}\,s^{-1}$ are shown alongside those for the stronger vorticity range of $\omega > 7 \times 10^{-5}\,s^{-1}$ used in Grandey et al. (2011). These median composites are constructed by calculating the median of the positive data within each storm-centric grid box. The weaker vorticity range was chosen to sample a similar number of storms to the stronger vorticity range. To provide an indication of the data spread within each of these vorticity ranges, lower and upper quartile composites are produced to complement the median composites. For example, Fig. 1 shows the τ composites for the North Atlantic ocean (NA). Figure 2 shows the corresponding f_c composites. The median storm-centre mean sea level pressures are 1008 hPa for the weaker range and 988 hPa for the stronger range.

2.4 Investigating the contribution of storm strength to observed cloud–aerosol relationships at each location in the storm-centric domain

The question mentioned in Sect. 1 is considered from two different perspectives in this paper. First, the contribution of ω to observed cloud–aerosol relationships is investigated at each individual grid box in the storm-centric domain. Second, the combined contribution of ω and storm spatial structure to observed cloud–aerosol relationships across the domain is investigated. The method used to investigate the former is outlined below; the method for the latter is discussed in the next section.

Regression slopes and correlations of the cloud-related properties versus τ are calculated at each 200 km × 200 km grid box in the domain for the all-conditions data and for the storm-centric data. The full range of vorticities, $\omega >$

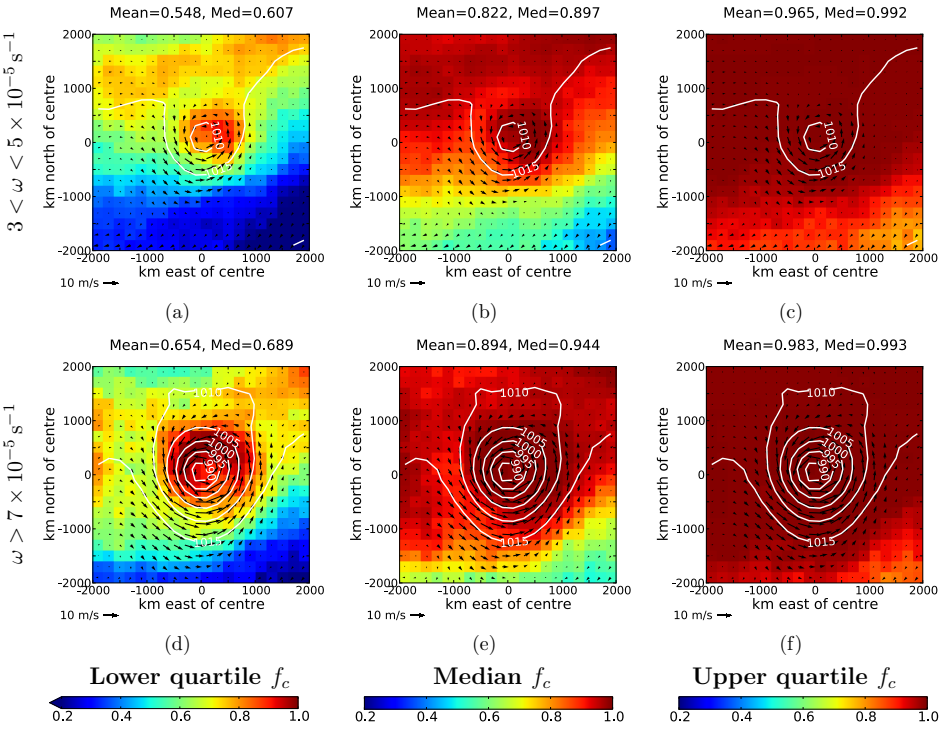

Fig. 2. Similar to Fig. 1, but for Aqua-MODIS cloud fraction (f_c) over the North Atlantic ocean.

$1\times10^{-5}\,s^{-1}$, are used for the regression and correlation calculations. Only positive aerosol and cloud data greater than zero are used. Linear fits are used for T_{top} versus τ and for f_c versus $\ln\tau$ based on semi-empirical considerations, including analysis of the coefficient of determination (Chapter 3 of Grandey, 2011). For example, the regression slopes and correlations of NA f_c versus $\ln\tau$ are shown in the first and third columns in Fig. 3.

In order to investigate the extent to which storm strength may be able to explain the observed relationships, the τ and cloud property data are shuffled for each grid box within narrow vorticity ranges of $1\times10^{-5}\,s^{-1}$ before recalculating the regression slopes and correlations. By randomising the pairing of the cloud and τ data before calculating the relationships, the contributions due to retrieval errors and aerosol–cloud interactions are largely removed. However, they may not be completely removed because some correctly matched cloud property and τ pairs may remain after shuffling, most likely for stronger storms with $\omega > 10\times10^{-5}\,s^{-1}$ where there are fewer storms in a given $1\times10^{-5}\,s^{-1}$ interval (Table 1). The shuffling occurs within narrow ω ranges, so the shuffled cloud and τ data remain functions of ω. The shuffling occurs independently for each grid box, so the shuffled data remain functions of position in the storm-centric domain. Therefore the calculated relationships between shuffled τ and the cloud properties represent the synoptic component which can be explained by ω for a given position in the storm-centric domain. Of course, no strong relationships should be found for the shuffled all-conditions data which are also included as a control. For example, the second and fourth columns in Fig. 3 show the regression slopes

Table 1. Minimum, mean and maximum number of f_c–τ data pairs per storm-centric 200 km × 200 km grid box for different 850 hPa relative vorticity (ω) ranges over the North Atlantic ocean.

ω range ($\times10^{-5}\,s^{-1}$)	Number of f_c–τ data pairs per grid box		
	Minimum	Mean	Maximum
1–2	59	132.3	172
2–3	110	253.5	338
3–4	129	285.2	378
4–5	143	243.0	308
5–6	132	239.6	303
6–7	81	165.2	219
7–8	42	113.9	151
8–9	19	58.7	88
9–10	8	32.7	54
10–11	3	15.7	35
11–12	2	9.2	23
12–13	0	0.1	1
13–14	0	0.0	0
all	899	1549.2	1880
3–5	272	528.2	667
> 7	94	230.4	311

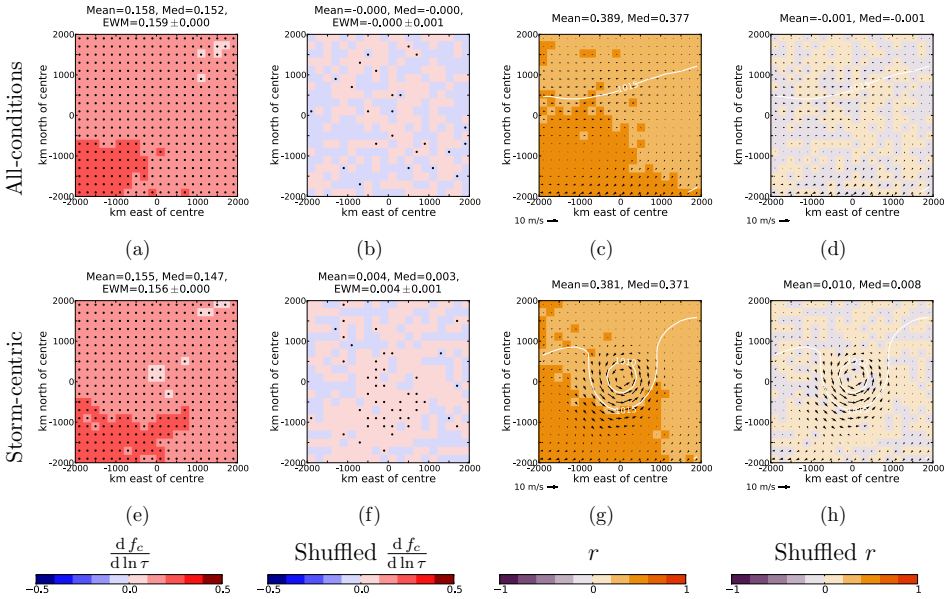

Fig. 3. (a) All-conditions results of an ordinary least squares regression fit of Aqua-MODIS cloud fraction (f_c) versus ln aerosol optical depth ($\ln\tau$) over the North Atlantic ocean. **(b)** Similar to **(a)**, but for f_c and $\ln\tau$ data which have been shuffled within each narrow relative vorticity range. Stippled slopes are statistically significant for a t test two-tailed p value threshold of 0.05. **(c)** Linear Pearson correlation coefficients (r) corresponding to the slopes shown in **(a)**. Median composites of ERA-Interim mean sea level pressure (p_0; white contours) and wind vectors (black arrows) are over-plotted. **(d)** Correlation coefficients corresponding to the slopes of the shuffled data shown in **(b)**. **(e–g)** Similar to **(a–d)**, but for storm-centric data rather than all-conditions data.

and correlations of NA f_c versus τ, where the data were first shuffled within each narrow vorticity range.

2.4.1 Investigating the combined contribution of storm strength and storm spatial structure to cloud–aerosol relationships across the storm-centric domain

In addition to calculating the regression slopes and correlations at each individual grid box in the domain, the slopes and correlations can also be calculated for the domain as a whole using all the data across the domain. By calculating the relationships for the shuffled data, the combined contribution of ω and storm spatial structure can be investigated. For comparison, the relationships can also be calculated for the median composites. For example, Table 2 shows the f_c–$\ln\tau$ results. The number of contributing data points varies slightly between the shuffled and non-shuffled data. This is due to the fact that the data are sometimes equal to zero, while only positive data are used for calculating the regression slopes and correlations.

3 Results and discussion

3.1 Aerosol optical depth (τ)

3.1.1 Composites of τ

Figure 1a–c shows the lower quartile, median and upper quartile storm-centric composites of Aqua-MODIS Collection 5 aerosol optical depth (τ) for North Atlantic ocean (NA) storms with relative vorticity in the range $3 < \omega < 5\times10^{-5}\,\mathrm{s}^{-1}$. The lower quartile composite has low τ across most of the domain, with a slight enhancement in the region of high wind speeds to the south-east of the storm centre. There is also a slight enhancement in the south-east corner of the domain, far away from the storm-centre, most likely due to background conditions in the NA. In the median composite, a slight enhancement is also visible just to the south-east of the storm centre, but is weak compared to the background. A decrease in the south-western and northern parts of the domain is visible in the median composite, likely due in part to the low wind speeds here, although frontal clearance via wet scavenging, subsidence behind the front and the advection of polar air may also play a role. This decrease is more striking in the upper quartile composite, showing that high τ values are uncommon to the north-west of the storm centre and in the south-western part of the domain for this vorticity range.

Figure 1d–f shows corresponding composites for a stronger vorticity range of $\omega > 7\times10^{-5}\,\mathrm{s}^{-1}$. A strong

Table 2. Number of data points, slopes, standard errors on the slopes and correlations for ordinary least squares regression fits of Aqua-MODIS cloud fraction (f_c) versus ln aerosol optical depth ($\ln\tau$) for different all-conditions and storm-centric data sets and 850 hPa relative vorticity (ω) ranges over the North Atlantic ocean. Slopes shown in italics are statistically significant for a t test two-tailed p value threshold of 0.05.

Data set	ω range ($\times10^{-5}$ s^{-1})	Number of points	Slope	Standard error	Correlation
All-conditions median composite	all	400	*−0.844*	0.112	−0.354
Storm-centric median composite	all	400	−0.173	0.090	−0.096
	3–5	400	−0.073	0.091	−0.040
	> 7	400	*0.156*	0.030	0.254
All-conditions	all	613913	*0.156*	0.000	0.377
Storm-centric	all	619675	*0.154*	0.000	0.369
	3–5	211266	*0.153*	0.001	0.365
	> 7	92150	*0.149*	0.001	0.377
All-conditions shuffled	all	609677	*−0.005*	0.001	−0.012
Storm-centric shuffled	all	615589	0.001	0.001	0.002
	3–5	209789	−0.001	0.001	−0.002
	> 7	91726	*0.016*	0.001	0.040

enhancement of τ in the regions of high wind speed to the south and east of the storm centre is visible in both the lower quartile and the upper quartile composites in addition to the median composite. This enhancement is due to a combination of wind speed dependent surface brightness artefacts and increased emission of sea salt (Grandey et al., 2011). The enhancement is much stronger for the stronger vorticity range than it is for the weaker vorticity range.

For both vorticity ranges, there is an average τ increase of approximately 0.05 between the lower quartile and median composites, and an increase of approximately 0.07 between the median and the upper quartile composites. This is quite a large spread compared to the average enhancement of less than 0.01 due to the change in vorticity. However, near the centre of the storm domain, the signal due to the vorticity change is approximately 0.05, comparable to the average differences between the medians and the quartiles.

The corresponding South Atlantic ocean composites can be seen in Fig. S1 of the Supplement. The latitudes have been inverted, with the poleward (southward) direction pointing to the top of the page. The results are similar to those obtained for the NA, but with a lower background τ level (Grandey et al., 2011).

3.2 Cloud fraction (f_c)

3.2.1 Composites of f_c

The lower quartile, median and upper quartile storm-centric composites of Aqua-MODIS Collection 5 cloud fraction for storms with vorticity in the range $3 < \omega < 5\times10^{-5}$ s^{-1} are shown in Fig. 2a–c. Blue indicates low f_c while red indicates high f_c. It can be seen there are often very high f_c values in the polewards part and the centre of the storm domain. Even in the lower quartile, f_c values larger than 0.8 are observed towards the centre of the storm domain. This feature corresponds to the cloud shield with cold T_{top} commented on in Sect. 3.3 below. In the upper quartile, the entire domain contains large f_c values, with the upper quartile composite domain mean being 0.965.

It is worth noting that these large fractional cloud covers may affect τ data in two ways. First, no aerosol retrievals will occur for grid boxes with complete cloud cover, biasing the τ data towards situations with lower f_c values. This is because aerosol retrievals require cloud-free pixels. Second, cloud contamination of τ may be correlated with f_c. However, the τ composites do not show a general meridional gradient in τ, only an enhancement near the storm centre, whereas the f_c composites show a strong meridional gradient. This suggests that potential cloud contamination alone cannot explain the observed τ composites shown in Fig. 1. However, it is possible that cloud contamination may still contribute towards observed relationships between aerosol and cloud-related properties, as discussed in Grandey et al. (2013).

Figure 2d–f shows the lower quartile, median and upper quartile storm-centric f_c composites for the stronger vorticity range of $\omega > 7\times10^{-5}$ s^{-1}. It can be seen from the mean sea level pressure contours, shown in white, that deeper pressure minima occur for these stronger storms. These composites

have similar spatial patterns to those for the weaker vorticity range, but with higher values of f_c. The domain mean f_c differences between the two vorticity ranges are approximately 0.1, 0.07 and 0.02 for the lower quartile, median and upper quartile composites respectively. This shows that storm strength can have a large effect on f_c. However, the domain mean differences between the lower quartile and the median, approximately 0.2–0.3, and between the median and upper quartile, approximately 0.1, show that there is also a large variation within each of these vorticity ranges. The SA f_c composites (not shown) are very similar to those for the NA.

It has been demonstrated that both τ and f_c generally increase with storm strength, suggesting that the large-scale synoptic conditions of extratropical cyclones may lead to relationships between these two variables. However, it has also been demonstrated that the variability of these variables is large, as shown by the differences between the quartile composites. Quantitative relationships between τ and f_c are now investigated.

3.2.2 The contribution of storm strength to f_c–$\ln\tau$ relationships at each location in the storm-centric domain

Figure 3a shows the all-conditions regression slopes of f_c versus $\ln\tau$. Positive slopes, shown in red, are observed everywhere in the all-conditions domain. Every grid box has a statistically significant f_c versus $\ln\tau$ regression slope, as shown by the ubiquitous stippling.

The corresponding storm-centric regression slopes, shown in Fig. 3e, are similarly significant. As mentioned in Sect. 2, the full vorticity range of all tracked storms is used. The storm-centric regression slopes are very similar to those for all-conditions. There is a slight weakening in the centre of the storm domain, possibly due to there being little variation in the high f_c values found here. The error-weighted mean (EWM) is only slightly smaller, being 0.156 compared to 0.159. The errors on these EWMs are more than two orders of magnitude smaller than the EWMs themselves.

As outlined in Sect. 2, the f_c and τ data are next shuffled within each grid box and vorticity range of $1\times10^{-5}\,s^{-1}$. The regression slopes for each grid box are then recalculated across the full vorticity range. The NA all-conditions results are shown in Fig. 3b. A mixture of positive and negative slopes are observed. The random shuffling largely removes correlations between f_c and τ induced by indirect effects and correlated retrieval errors. The simplified large-scale synoptic contribution described by ω and position in the storm domain is retained. Since ω and position are meaningless references for the all-conditions data, it should be expected that the shuffled all-conditions slopes should be approximately zero. The magnitude of the EWM is smaller than the one-sigma standard error. Furthermore, it is more than two orders of magnitude smaller than the all-conditions EWM for the non-shuffled data.

Figure 3f shows the regression slopes for the shuffled NA storm-centric data. Many individual slopes just to the south and west of the domain centre are positive and significant, suggesting that the simplified description of the large-scale synoptics investigated here may indeed explain a contribution to observed relationships between f_c and τ. This part of the domain, to the south of the storm centre, is also where the winds are strongest. The significant EWM of 0.004, which is an order of magnitude larger than the shuffled all-conditions EWM, also supports this suggestion. However, this EWM is still almost two orders of magnitude smaller than the non-shuffled EWM of 0.156.

Similar observations can be made for the f_c–$\ln\tau$ correlation coefficients. The all-conditions and storm-centric correlation coefficients, shown in Fig. 3c and g, are very similar to each other and are consistently positive. The correlations for the shuffled NA all-conditions f_c and $\ln\tau$ data, shown in Fig. 3d, are more than two orders of magnitude smaller. The mean of -0.001 has an opposite sign to that for the non-shuffled all-conditions data and is close to zero, consistent with the regression slopes. The correlations for the shuffled storm-centric data, shown in Fig. 3h, are mostly positive, particularly near the storm centre. The mean of 0.010 is stronger than that for the shuffled all-conditions data, but it is still much smaller than the correlations for the non-shuffled data.

The f_c–$\ln\tau$ regression slope and correlation results for the SA are shown in Fig. S2 of the Supplement. The latitudes have been inverted. One difference compared to the NA is that there is a stronger meridional gradient in the regression slopes. Apart from this difference, the results are very similar to those for the NA.

In this section, the contribution of ω, a measure of storm strength, to f_c–$\ln\tau$ relationships at each location in the storm-centric domain has been investigated. For the shuffled storm-centric data, statistically significant EWM regression slopes have been found, suggesting that storm strength may, to some extent, drive relationships between T_{top} and τ via meteorology. This effect appears to be stronger near the centre of the storm. However, the relationships for the shuffled data are generally much weaker than those for the non-shuffled data, demonstrating that the contribution explained by storm strength is only a small component of the observed relationships.

3.2.3 The combined contribution of storm strength and storm spatial structure to f_c–$\ln\tau$ relationships across the storm-centric domain

Looking at the median composites for the stronger storm strength range of $\omega > 7\times10^{-5}\,s^{-1}$, Figs. 1e and 2e, it appears that the τ and f_c medians are spatially correlated, with higher τ and f_c values near the centre of the storm-centric domain. This is indeed the case, with the f_c–$\ln\tau$ correlation coefficient being 0.254 between these median composites (Table 2). The corresponding regression slope is 0.156.

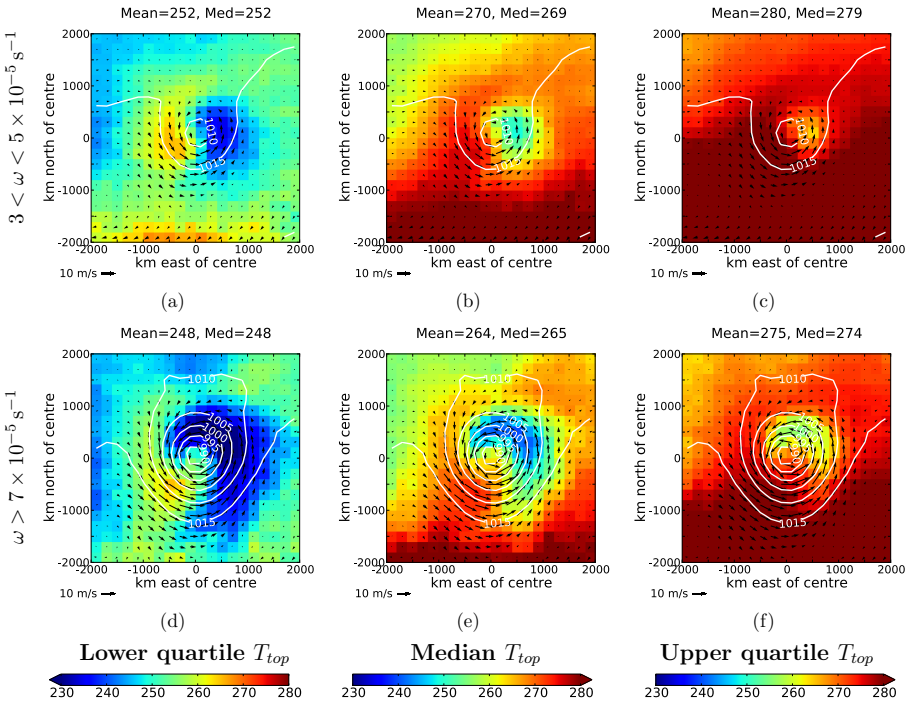

Fig. 4. Similar to Fig. 1, but for Aqua-MODIS cloud top temperature (T_{top}, K) over the North Atlantic ocean.

However, if the median composites for the weaker vorticity range or for all storms are used, the slopes and correlations become negative. For the all-conditions median composite, the slope is also negative, probably due to a spatial gradient effect (Grandey and Stier, 2010).

When all the all-conditions data, rather than just the medians, are used, the regression slope is 0.156, similar to the EWM of the regression slopes calculated for each grid box in the previous session. For the storm-centric data, the regression slopes are very similar, varying in the range 0.149–0.154 depending on the ω range used. It is remarkable that the regression slope for the storm-centric median composite for the stronger ω range, 0.156, is so similar to these values. However, it would incorrect to conclude that the storm-centric spatial correlation is responsible for the observed f_{c}–$\ln\tau$ relationships. This is because variability is not taken into account when the median composites are used.

In order to account for variability, the regression slopes and correlations are calculated using all the shuffled data. The slope for the all-conditions shuffled data is -0.005, weakly negative and statistically significant. The significance may be due to either a spatial gradient effect or a statistical artefact. For the weaker and full ω ranges, the slopes for the storm-centric shuffled data are insignificant. The slope for the stronger vorticity range, 0.016, is significant and larger than the all-conditions slope. However, it is still much smaller than the slopes for the non-shuffled data.

In this section, the combined contribution of ω and storm spatial structure to f_{c}–$\ln\tau$ relationships has been investigated. Insignificant regression slopes are found when data for the weaker ω range or the full ω range are used. On the other hand, a significant regression slope is found when the stronger ω range is used. However, as in the previous section, the f_{c}–$\ln\tau$ relationships explained are far smaller than the observed relationships. This demonstrates that the contribution explained by ω and storm spatial structure represents only a very small component of the observed relationships.

3.3 Cloud top temperature (T_{top})

3.3.1 Composites of T_{top}

Figure 4a–c shows the lower quartile, median and upper quartile storm-centric composites of Aqua-MODIS Collection 5 cloud top temperature (T_{top}) for NA storms with relative vorticity in the range $3 < \omega < 5\times10^{-5}\,\mathrm{s}^{-1}$. The lower quartile tends towards sampling scenes where cold, high clouds dominate, whereas the upper quartile tends towards scenes where warm, low clouds can be seen. A shield of colder, higher clouds can be discerned to the east of the storm centre in all three of the composites. Relatively cold clouds can also be seen in the advected cold polar air in the north-west of the storm-centric domain. In the lower quartile, a band of warmer clouds can be seen to the west of the storm centre, indicating a general absence of high clouds here. A general meridional gradient in T_{top} exists, with warmer clouds generally observed at the equatorward edge of the domain.

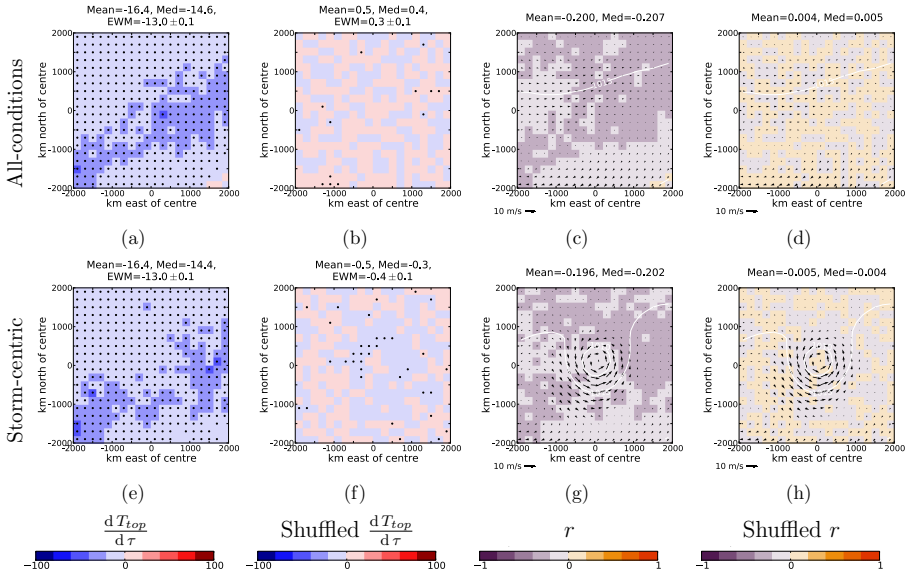

Fig. 5. Similar to Fig. 3, but for ordinary least squares regression fits of cloud top temperature (T_{top}, K) versus aerosol optical depth (τ) over the North Atlantic ocean.

Table 3. Similar to Table 2, but for but for ordinary least squares regression fits of cloud top temperature (T_{top}, K) versus aerosol optical depth (τ) over the North Atlantic ocean.

Data set	ω range ($\times 10^{-5}\,\mathrm{s}^{-1}$)	Number of points	Slope (K)	Standard error (K)	Correlation
All-conditions median composite	all	400	*405.7*	45.2	0.410
Storm-centric median composite	all	400	−23.0	35.3	−0.033
	3–5	400	−67.1	34.3	−0.098
	> 7	400	*−79.2*	15.6	−0.246
All-conditions	all	612480	*−13.3*	0.1	−0.172
Storm-centric	all	618025	*−14.0*	0.1	−0.175
	3–5	210697	*−15.6*	0.2	−0.191
	> 7	91991	*−16.1*	0.3	−0.204
All-conditions shuffled	all	615772	*0.7*	0.1	0.007
Storm-centric shuffled	all	621833	*−0.7*	0.1	−0.007
	3–5	212007	*−1.0*	0.2	−0.010
	> 7	92302	*−2.3*	0.3	−0.022

The composites for the stronger vorticity range of $\omega > 7\times10^{-5}\,\mathrm{s}^{-1}$ are shown in Fig. 4d–f. These composites have similar general features to those for the weaker vorticity range. The shield of cold, high clouds is larger and colder for the stronger vorticity range than it is for the weaker vorticity range. This is to be expected, since this shield of high clouds is synoptically driven.

Field and Wood (2007) presented a NA T_{top} mean composite plot. They used a different storm identification and compositing methodology to that used here, identifying extratropical cyclones based on surface pressure gradients and minima. Their mean composite of T_{top} has similar features to the median composites produced here and shown in Fig. 4. The T_{top} values of the Field and Wood (2007) composite are somewhere between those for the two vorticity ranges used here. Similarly, their mean storm-centre mean sea level pressure of approximately 1000 hPa is between the median storm-centre values of 1008 hPa and 988 hPa for the NA composites produced here.

For both vorticity ranges, the domain average increase in T_{top} between the lower quartile and the median is approximately 17 K. The increase between the median and the upper quartile is approximately 10 K. The domain average decrease between the weaker composites and the stronger composites is approximately 5 K, considerably smaller than the spread between the quartiles. However, the strengthening of the high cloud shield can result in some grid boxes seeing decreases of up to 20 K. The SA T_{top} composites (not shown) are very similar to those for the NA.

3.3.2 The contribution of storm strength to T_{top}–τ relationships at each location in the storm-centric domain

Figure 5a shows the regression slopes of T_{top} versus τ for each grid box of the NA all-conditions gridded data. It can be seen that negative regression slopes, indicated by blue, are found almost everywhere in the domain. Almost all of these regression slopes are statistically significant, indicated by the stippling. The EWM for the whole domain, -13.0 K, is two orders of magnitude larger than the associated one-sigma error.

The corresponding storm-centric regression slopes are shown in Fig. 5e. It can be seen that the storm-centric regression slopes are very similar to those for all-conditions. The storm-centric EWM of -13.0 K is almost identical to the all-conditions EWM. This shows that analysing relationships between NA T_{top} and τ in a storm-centric context appears to make little discernible difference to the results.

As outlined in Sect. 2, the T_{top} and τ data are then shuffled for each grid box within narrow vorticity ranges of 1×10^{-5} s^{-1}. The regression slopes are then recalculated. It would be expected that these regression slopes for the shuffled all-conditions data should be statistically indistinguishable from zero. This is indeed the case for most grid boxes, as indicated by the lack of stippling across most of the domain in Fig. 5b. However, the shuffled all-conditions slope EWM of 0.3 K is larger than the one-sigma standard error of 0.1 K. This is likely to be an artefact. It is worth noting that the EWM is two orders of magnitude smaller than for the non-shuffled data, and is positive rather than negative.

The slopes for the shuffled storm-centric data, shown in Fig. 5f, are also very small. A few of the regression slopes are significant, particularly near the centre of the storm-centric domain. The EWM of -0.4 K is only slightly larger in magnitude than that of the shuffled all-conditions data control. The similarity in size between these two EWMs means that caution should be applied when interpreting the significance of the shuffled storm-centric EWMs. As with the f_c–$\ln\tau$ results, the shuffled storm-centric EWM is much smaller than EWM of -13.0 K for the non-shuffled data.

The all-conditions and storm-centric correlation coefficients, shown in Fig. 5c and g, are also very similar to one another. The observed correlations are negative, approximately -0.2 on average. The correlations for the shuffled all-conditions and storm-centric data are shown in Fig. 5d and h. They are two orders of magnitude smaller than for the non-shuffled data. These observations for the correlation coefficients are consistent with those made for the regression slopes.

Regression slopes and correlations for the SA are shown in Fig. S3 of the Supplement. There is a stronger meridional gradient in the SA, with the slopes becoming steeper nearer the Equator. As was the case for the NA results, the all-conditions and storm-centric EWM regression slopes are very similar. The SA shuffled all-conditions regression slope EWM of 0.1 K is statistically insignificant in the SA, unlike that for the NA. The SA shuffled storm-centric slope EWM of -0.5 K is larger and significant. However, the EWM is still much smaller than that of the of the non-shuffled data.

The interpretation of these results is similar to the corresponding interpretation of the f_c–$\ln\tau$ results in Sect 3.2.2. A few statistically significant regression slopes have been found, suggesting that storm strength may, to some extent, drive relationships between T_{top} and τ via meteorology. This effect appears to be slightly more robust near the centre of the storm-centric domain. However, the relationships for the shuffled data are generally much weaker than those for the non-shuffled data, demonstrating that the contribution explained by ω is only a very small component of the observed relationships.

3.3.3 The combined contribution of storm strength and storm spatial structure to T_{top}–τ relationships across the storm-centric domain

The combined contribution of ω and storm spatial structure is now investigated. The analysis method is the same as that used to investigate f_c–$\ln\tau$ relationships in Sect. 3.2.3. The regression slopes for the T_{top}–τ data sets are shown in Table 3.

When all data is used, the all-conditions regression slope is -13.3 K, similar to the EWMs for the non-shuffled data calculated in the previous section. The storm-centric regression slopes vary in the range -14.0 to -16.1 K, depending on the ω range used.

For the all-conditions median composites, a large positive regression slope of 405.7 K is found, showing a strong spatial gradient effect. The regression slopes are insignificant for the weaker ω and all ω storm-centric median composites. However, there is a significant spatial correlation for the stronger ω composites, leading to a strongly negative regression slope of -79.2 K.

When all the all-conditions shuffled data are used, a significant positive slope of 0.7 K is found, likely due to a spatial gradient effect or a statistical artefact. The regression slopes for the storm-centric shuffled data vary from -0.7 K (all ω) to -2.3 (stronger ω, $> 7\times10^{-5}$ s^{-1}). These slopes are

an order of magnitude smaller than those found for the non-shuffled data.

The interpretation is similar to that proposed for the f_c–$\ln\tau$ results in Sect 3.2.3. The combined contribution of ω and storm spatial structure can explain only a small component of observed T_{top}–τ relationships.

4 Conclusions

In Grandey et al. (2011), it was shown that extratropical cyclones affect Aqua-MODIS retrieved aerosol optical depth (τ) over ocean. This paper has further demonstrated that on average for a given position in the storm-centric domain, stronger storms generally lead to higher τ than weaker storms, particularly near the storm centre. However, this enhancement is generally smaller than the variability in τ for a given storm strength and position in the storm-centric domain, probably due to variations in local wind speeds.

Storm-centric composites of cloud-related properties have been investigated in this paper, building on the previous work of Lau and Crane (1995, 1997), Norris and Iacobellis (2005), Wang and Rogers (2001), Chang and Song (2006), Field and Wood (2007) and Field et al. (2008). Median composites of cloud fraction (f_c) show a general increase in f_c with storm strength. However, as for the τ fields, the variability between the quartiles for a given storm strength is generally larger than the difference between different storm strengths.

Cloud top temperature (T_{top}) composites reveal a cold, high cloud shield to the north and east of the storm centre. The extent and height of this shield increases with storm strength. The domain average T_{top} is colder for stronger storms compared to weaker storms. However, once again the variability between the quartiles for a given storm strength is generally larger than the difference due to vorticity changes, except for some grid boxes near the centre of the storm domain.

Because storm strength has been shown to affect τ, f_c and T_{top}, it seemed plausible to hypothesise that extratropical cyclones may drive relationships between these three properties. Storm-centric regression slopes and correlation coefficients of f_c versus $\ln\tau$ and T_{top} versus τ have been calculated. Positive f_c–$\ln\tau$ and negative T_{top}–τ relationships are observed.

The τ, f_c and T_{top} data have subsequently been shuffled within narrow ranges of storm vorticity, prior to recalculating the regressions slopes and correlations. This has been done in an attempt to remove correlations due to retrieval errors and genuine aerosol–cloud interactions. By choosing narrow ranges of storm vorticity and retaining position in the storm domain, a simplified description of the large-scale synoptics of extratropical cyclones has been investigated. This has been done in order to answer the question asked at the beginning of the paper: can relationships between aerosol and cloud-related properties be explained by considering simply the relative vorticity of extratropical cyclones and position relative to the storm centre? This question has been considered from two perspectives. First, the contribution of ω to observed cloud–aerosol relationships has been investigated at each individual grid box in the storm-centric domain. Second, the combined contribution of ω and storm spatial structure to observed cloud-aerosol relationships across the domain has been investigated.

For both approaches, the f_c versus $\ln\tau$ regression slopes for the shuffled data are often found to be significant. This suggests that the storm strength and spatial structure can, to some extent, explain relationships between f_c and τ. However, these relationships are far smaller than observed relationships between f_c and τ, which may be better explained by cloud contamination, relative humidity (Quaas et al., 2010; Chand et al., 2012; Grandey et al., 2013) and descriptions of meteorology based on local field variables such as winds (Engström and Ekman, 2010). Many of the significant slopes are found just to the south of the storm centre, where the winds are generally strongest. This suggests that the synoptically induced winds, which were largely found to explain the observed storm-centric τ composites (Grandey et al., 2011), may be the mechanism by which the storm-centric large-scale synoptics can explain relationships between f_c and τ.

The T_{top} versus τ regression slopes for the shuffled data are also often found to be significant but much smaller than the observed relationships for the non-shuffled data. The conclusions are similar to those for the f_c–τ relationships. The description of storm strength and storm spatial structure used in this paper can explain only a small component of observed T_{top}–τ relationships. Further research is needed to identify the contributions of satellite retrieval errors, local meteorology and aerosol–cloud interactions to observed T_{top}–τ relationships.

As an alternative to using local meteorological field variables to account for relationships between aerosol and cloud-related properties, this paper has introduced the possibility of considering large-scale synoptic systems instead. The approach used, whereby data are categorised according to position in the storm-centric domain and storm vorticity, has proved to be partially successful. A combination of the storm-centric and local meteorological variable approaches might be more fruitful than either approach taken in isolation. Cloud and aerosol data could be categorised by both position in the storm-centric domain and a local meteorological variable, providing a basis for future work. A complementary approach may be to consider cloud regimes, as has been done by Gryspeerdt and Stier (2012) for the investigation of relationships between liquid cloud droplet number concentration and τ.

Supplementary material related to this article is available online at http://www.atmos-chem-phys.net/13/10689/2013/acp-13-10689-2013-supplement.pdf.

Acknowledgements. MODIS data were obtained from the Level 1 and Atmosphere Archive and Distribution System (LAADS). ERA-Interim data were obtained from the European Centre for Medium-Range Weather Forecasts (ECMWF). The TRACK code and configuration were provided by Kevin Hodges. This work was supported by a UK Natural Environment Research Council (NERC) DPhil studentship and also the NERC AEROS project (NE/G006148/1). The research leading to these results has also received funding from the European Research Council under the European Union's Seventh Framework Programme (FP7/2007–2013)/ERC grant agreement no. FP7-280025. R. G. Grainger acknowledges funding from the NERC National Centre for Earth Observation. B. S. Grandey acknowledges funding from the Singapore National Research Foundation (NRF) through the Singapore-MIT Alliance for Research and Technology (SMART) Center for Environmental Sensing and Modeling (CENSAM). Thanks are due to Joanna Eberhardt, three anonymous referees and the editor for providing helpful comments.

Edited by: T. J. Dunkerton

References

Anderson, T. L., Charlson, R. J., Winker, D. M., Ogren, J. A., and Holmén, K.: Mesoscale variations of tropospheric aerosols, J. Atmos. Sci., 60, 119–136, 2003.

Andreae, M. O., Jones, C. D., and Cox, P. M.: Strong present-day aerosol cooling implies a hot future, Nature, 435, 1187–1190, doi:10.1038/nature03671, 2005.

Chand, D., Wood, R., Ghan, S. J., Wang, M., Ovchinnikov, M., Rasch, P. J., Miller, S., Schichtel, B., and Moore, T.: Aerosol optical depth increase in partly cloudy conditions, J. Geophys. Res., 117, D17207, doi:10.1029/2012JD017894, 2012.

Chang, E. K. M. and Song, S.: The seasonal cycles in the distribution and precipitation around cyclones in the Western North Pacific and Atlantic, J. Atmos. Sci., 63, 815–839, 2006.

Engström, A. and Ekman, A. M. L.: Impact of meteorological factors on the correlation between aerosol optical depth and cloud fraction, Geophys. Res. Lett., 37, L18814, doi:10.1029/2010GL044361, 2010.

Field, P. R. and Wood, R.: Precipitation and cloud structure in midlatitude cyclones, J. Climate, 20, 233–254, doi:10.1175/JCLI3998.1, 2007.

Field, P. R., Gettelman, A., Neale, R. B., Wood, R., Rasch, P. J., and Morrison, H.: Midlatitude cyclone compositing to constrain climate model behaviour using satellite observations, J. Climate, 21, 5887–5903, doi:10.1175/2008JCLI2235.1, 2008.

Forster, P., Ramaswamy, V., Artaxo, P., Berntsen, T., Betts, R., Fahey, D. W., Haywood, J., Lean, J., Lowe, D. C., Myhre, G., Nganga, J., Prinn, R., Raga, G., Schultz, M., and Van Dorland, R.: Changes in atmospheric constituents and in radiative forcing, in: Climate Change 2007: The Physical Science Basis. Contribution of Working Group 1 to the Fourth Assessment Report of the Intergovernmental Panel on Climate Change, Cambridge University Press, 129–234, 2007.

Grandey, B. S. and Stier, P.: A critical look at spatial scale choices in satellite-based aerosol indirect effect studies, Atmos. Chem. Phys., 10, 11459–11470, doi:10.5194/acp-10-11459-2010, 2010.

Grandey, B. S.: Investigating aerosol–cloud interactions, Ph.D. thesis, University of Oxford, UK, available at: http://ora.ox.ac.uk/objects/uuid:8b48c02b-3d43-4b04-ae55-d9885960103d, 2011.

Grandey, B. S., Stier, P., Wagner, T. M., Grainger, R. G., and Hodges, K. I.: The effect of extratropical cyclones on satellite-retrieved aerosol properties over ocean, Geophys. Res. Lett., 38, L13805, doi:10.1029/2011GL047703, 2011.

Grandey, B. S., Stier, P., and Wagner, T. M.: Investigating relationships between aerosol optical depth and cloud fraction using satellite, aerosol reanalysis and general circulation model data, Atmos. Chem. Phys., 13, 3177–3184, doi:10.5194/acp-13-3177-2013, 2013.

Gryspeerdt, E. and Stier, P.: Regime-based analysis of aerosol-cloud interactions, Geophys. Res. Lett., 39, L21802, doi:10.1029/2012GL053221, 2012.

Hodges, K. I.: Feature tracking on the unit sphere, Mon. Weather Rev., 123, 3458–3465, 1995.

Hodges, K. I.: Adaptive constraints for feature tracking, Mon. Weather Rev., 127, 1362–1373, 1999.

Hodges, K. I., Lee, R. W., and Bengttson, L.: A Comparison of Extratropical Cyclones in Recent Reanalyses ERA-Interim, NASA MERRA, NCEP CFSR, and JRA-25, J. Climate, 24, 4888–4906, doi:10.1175/2011JCLI4097.1 2011.

Kaufman, Y. J., Koren, I., Remer, L. A., Rosenfeld, D., and Rudich, Y.: The effect of smoke, dust, and pollution aerosol on shallow cloud development over the Atlantic Ocean, P. Natl. Acad. Sci. USA, 102, 11207–11212, doi:10.1073/pnas.0505191102, 2005.

Kiehl, J. T.: Twentieth century climate model response and climate sensitivity, Geophys. Res. Lett., 34, L22710, doi:10.1029/2007GL031383, 2007.

Koren, I., Kaufman, Y. J., Rosenfeld, D., Remer, L. A., and Rudich, Y.: Aerosol invigoration and restructuring of the Atlantic convective clouds, Geophys. Res. Lett., 32, L14828, doi:10.1029/2005GL023187, 2005.

Lau, N.-C. and Crane, M. W.: A satellite view of the synoptic-scale organization of cloud properties in midlatitude and tropical circulation systems, Mon. Weather Rev., 123, 1984–2006, 1995.

Lau, N.-C. and Crane, M. W.: Comparing satellite and surface observations of cloud patterns in synoptic-scale circulation systems, Mon. Weather Rev., 125, 3172–3189, 1997.

Lohmann, U. and Feichter, J.: Global indirect aerosol effects: a review, Atmos. Chem. Phys., 5, 715–737, doi:10.5194/acp-5-715-2005, 2005.

Norris, J. R. and Iacobellis, S. F.: North Pacific cloud feedbacks inferred from synoptic-scale dynamic and thermodynamic relationships, J. Climate, 18, 4862–4878, 2005.

Platnick, S., King, M. D., Ackerman, S. A., Menzel, W. P., Baum, B. A., Riedi, J. C., and Frey, R. A.: The MODIS cloud products: algorithms and examples from terra, IEEE T. Geosci. Remote, 41, 459–473, doi:10.1109/TGRS.2002.808301, 2003.

Quaas, J., Stevens, B., Stier, P., and Lohmann, U.: Interpreting the cloud cover – aerosol optical depth relationship found in satellite

data using a general circulation model, Atmos. Chem. Phys., 10, 6129–6135, doi:10.5194/acp-10-6129-2010, 2010.

Remer, L. A., Kaufman, Y. J., Tanré, D., Mattoo, S., Chu, D. A., Martins, J. V., Li, R.-R., Ichoku, C., Levy, R. C., Kleidman, R. G., Eck, T. F., Vermote, E., and Holben, B. N.: The MODIS Aerosol Algorithm, Products, and Validation, J. Atmos. Sci., 62, 947–973, doi:10.1175/JAS3385.1, 2005.

Stevens, B. and Feingold, G.: Untangling aerosol effects on clouds and precipitation in a buffered system, Nature, 461, 607–613, doi:10.1038/nature08281, 2009.

Wang, C.-C. and Rogers, J. C.: A composite study of explosive cyclogenesis in different sectors of the North Atlantic, Part I: Cyclone structure and evolution, Mon. Weather Rev., 129, 1481–1499, 2001.

Weigum, N. M., Stier, P., Schwarz, J. P., Fahey, D. W., and Spackman, J. R.: Scales of variability of black carbon plumes over the Pacific Ocean, Geophys. Res. Lett., 39, L15804, doi:10.1029/2012GL052127, 2012.